# Dual Antioxidant Properties and Organic Radical Stabilization in Cellulose Nanocomposite Films Functionalized by In Situ Polymerization of Coniferyl Alcohol

Élise Gerbin, Yves-Michel Frapart, Carlos Marcuello, Betty Cottyn, Laurence Foulon, Miguel Pernes, David Crônier, Michaël Molinari, Brigitte Chabbert, Paul-Henri Ducrot, et al.

Article

# Dual antioxidant properties and organic radical stabilization in cellulose nanocomposite films functionalized by *in situ* polymerization of coniferyl alcohol

Elise Gerbin, Yves-Michel Frapart, Carlos Marcuello, Betty Cottyn, Laurence Foulon, Miguel Pernes, David Crônier, Michael Molinari, Brigitte Chabbert, Paul-Henri Ducrot, Stéphanie Baumberger, Véronique Aguié-Béghin, and Bernard Kurek

*Biomacromolecules*, **Just Accepted Manuscript** • Publication Date (Web): 25 Jun 2020



## Just Accepted



is published by the American Chemical Society. 1155 Sixteenth Street N.W., Washington, DC 20036

# Dual antioxidant properties and organic radical stabilization in cellulose nanocomposite films functionalized by *in situ* polymerization of coniferyl alcohol

*Elise Gerbin†,‡, Yves-Michel Frapart#, Carlos Marcuello†, Betty Cottyn‡, Laurence Foulon†, Miguel Pernes†, David Cronier†, Michael Molinari§, Brigitte Chabbert†, Paul-Henri Ducrot‡, Stéphanie Baumberger‡, Véronique Aguié-Béghin†*, Bernard Kurek†*

† Université de Reims Champagne Ardenne, INRAE, FARE, UMR A 614, 51097 Reims, France

‡ Institut Jean-Pierre Bourgin, INRAE, AgroParisTech, CNRS, Université Paris-Saclay, 78000 Versailles, France

# Laboratoire de Chimie et Biochimie Pharmacologiques et Toxicologiques—UMR CNRS 8601, Université de Paris, France

§ CBMN UMR CNRS 5248, Université de Bordeaux, IPB, Pessac, 33600, France

KEYWORDS. Lignin, cellulose nanocrystals, Fenton oxidation, phenoxy radicals, nanomechanical properties, hygroscopic properties

ABSTRACT. A new biobased material based on an original strategy using lignin model compounds as natural grafting additive on a nanocellulose surface through *in situ* polymerization of coniferyl alcohol by the Fenton reaction at two pH values was investigated. The structural and morphological properties of the materials at the nanoscale were characterized by a combination of analytical methods, including Fourier transform infrared (FTIR) spectroscopy, liquid chromatography combined with mass spectrometry (LC-MS), nuclear molecular resonance (NMR) spectroscopy, electron paramagnetic resonance (EPR) spectroscopy, water sorption capacity by dynamic vapor sorption (DVS) and atomic force microscopy (AFM, topography and indentation modulus measurements). Finally, the usage properties, such as antioxidant properties, were evaluated in solution and from the nanostructured casted films by radical 2,2′-diphenyl-1-picrylhydrazyl (DPPH°) scavenging tests. We demonstrate the structure–function relationships of these advanced CNC-lignin films and describe their dual functionalities and characteristics, namely, their antioxidant properties and the presence of persistent phenoxy radicals within the material.

## Introduction

Explorations of diverse bioderived polymers and strategies for modifying and functionalizing these materials has inspired the design of new molecular assemblies. Interestingly, some of these materials exhibit unexpected properties, resulting in renewable carbon-based materials suitable for high value-added applications. Among these biopolymers, the major components of lignocellulosic biomass, cellulose, hemicelluloses and lignins, are of particular interest, both in terms of their properties and availability.

Cellulose, one of the most abundant biopolymers on earth, is widely used in paper fibers, and it is often used in the chemical industry in its polymerized or depolymerized form. In addition to these traditional applications, interest in cellulose nanocrystals (CNCs) or nanofibrils (CNFs) for the design of functional materials is very high due to the unique properties of cellulose at the nanoscale. The potential commercial uses of CNCs and CNFs are being recognized[1-3], and this is supported by industrial use, as up to 300 t of CNC$^{MC}$ CelluForce® is prepared per year[4]. The use of such cellulose-based nanoassemblies has attracted increased attention in various fields for a wide range of applications, including in film packaging as a filler material, as gas and water permeable barriers[5, 6], in iridescent paper[7], in tissue engineering in medical fields[8, 9], and in solar panels[10].

Industrial lignins are byproducts of the pulp and paper industry but are also generated by emerging biorefineries. In total, 50-70 million tons of lignins are generated per year with projections of more than a 3-fold increase by 2030[11]. Historically combusted to produce energy (Kraft lignins) or used as dispersants, plasticizers and fillers in many industrial sectors (lignosulfonates)[12], industrial lignins are also a source of biomolecules with potential in high value-added applications due to their phenolic structure and related specific properties[13]. Lignins are multifunctional compounds of interest for the design of new biopolymer-based materials. Depending on their nature, chemical composition and physical properties, they can

be used as fillers in composites[14], as aromatic substrates to produce carbon fibers[15, 16], and as antireflective, UV protective or antioxidative materials in nanostructured cellulose-based films[17-19].

In the most recent studies on lignocellulose-based nanocomposites, water or moisture resistance was desired to maintain the physical integrity of the material and achieve the necessary usage properties. Therefore, petroleum or bioderived hydrophobic matrices are generally preferred and developed[20, 21]. Thus, selective chemical processes to improve component reactivity and compatibility for preparing nanocomposites based on CNC and/or lignin have been studied.

CNCs extracted from plant sources (wood pulp, ramie, hemp, and flax fiber) are crystalline nanorods with a high specific surface area of approximately 465 $m^2/g$ [22] and an aspect ratio (length/diameter, L/d) of approximately 25-30. Their hydrophilicity, which is due to the large amount of hydroxyl and sulfate ester groups (estimated at 0.6 – 0.8%[23]) on the surface resulting from acid hydrolysis, makes them difficult to disperse in hydrophobic matrices. To use them in more hydrophobic matrices, CNCs can be functionalized by modification of the hydroxyl groups[21, 24], for example, by esterification, trans-esterification with carboxylic acids or esters such as caprolactones, carbamation with isocyanates, oxidation or silylation. These methods have also been used to graft macromolecules on to CNCs; the macromolecules used in such reactions include polyethylene glycol chains[20], poly-N-isopropylacrylamides (by radical polymerization in the presence of an initiator[25]), Jeffamine® polyetheramines (through peptidic coupling after TEMPO oxidation of the CNCs[26]) and lignins. For example, propargylated Kraft lignins were grafted onto azide-modified cellulose by click chemistry[27], and lignin oligomers were grafted onto CNCs by chemical oxidation with Fenton's reagent in an aqueous dioxane solvent[18]. These derivatizations with lignins give CNC nanoparticles and the final materials new properties including altering the hydrophobic/hydrophilic balance[28], thermoresponsiveness

in aqueous suspensions[26], waterproofness, UV absorption, antioxidant properties[18], mechanical properties and water sorption capacity of coated cellulose-based films[29].

Although interest in lignin grafting onto CNCs has been demonstrated, it was suggested that the *in situ* polymerization of aromatic precursors of lignin could also be an interesting way to build nanocomposites with new properties. Different strategies, such as physical mixtures of CNCs and lignin oligomers (dehydropolymer (DHP) or fractionated lignin)[19], enzymatic polymerization of coniferyl alcohol in the presence of CNC or hemicellulose[29, 30], or oxidation of a mixture of CNC and lignin oligomers by Fenton's reagent[17, 18], have been used to achieve these goals. The properties of these nanocomposites, including their hygroscopic, nanomechanical, antioxidant and UV barrier properties, can be modulated based on the assembly method and were characterized.

Fenton oxidation, a mixture of hydrogen peroxide and a ferrous salt that is generated along with hydroxyl radicals, is one of the most interesting pathways for building CNC-lignin nanocomposites. Indeed, this reaction generates ROS, a generic term for low-molecular-weight chemically reactive species containing oxygen. They are generally short-lived species such as hydroxyl (HO°), superoxide ($O_2^{\circ-}$), alkoxyl (RO°) or peroxyl (ROO°) radicals. Nonradical entities, such as hydrogen peroxide ($H_2O_2$), organic hydroperoxides (RCOOH) and hypochlorous acid (HOCl), are also considered ROS.

Hydroxyl radicals produced by Fenton's reagent are known to react with various lignin model compounds, promoting cleavage of β-O-4 bonds, demethoxylation and hydroxylation[31-34]. It was also shown that the Fenton reaction can either depolymerize or polymerize lignin[35] depending on the Fenton conditions used (pH and concentration are the major factors). It was also demonstrated that ROS can take part in the oxidative depolymerization of polysaccharides[36, 37] through the cleavage of glycosidic bonds[38, 39]. ROS are therefore reactive

species that can either produce or degrade materials composed of lignocellulosic polymers according to the conditions and the chemistry of the system under investigation.

In the present work, we investigated the use of highly reactive oxygenated species for the production of CNC-lignin-based materials. We have developed a strategy for grafting lignin oligomers on CNC surfaces through the *in situ* oxidation of coniferyl alcohol (CA) by Fenton reaction in a stable cellulose colloidal suspension. We characterized the structural and functional properties of the obtained structured films at the nanoscale using chemical and physicochemical methods. The formation of phenoxy radicals in the material, resulting from the action of hydroxyl radicals in the reaction medium, was also investigated. The produced data allow us to demonstrate the structure–function relationships of these advanced CNC-lignin films and to report their dual functionalities and characteristics, namely, antioxidant properties and the presence of persistent phenoxy radicals within the material.

## Experimental section

**Materials**: Cellulose nanocrystals (CNCs) were prepared by acid hydrolysis of ramie fibers (*Boehmeria nivea*) according to the procedure described by Hambardzumyan *et al.*[40]. The lignin model compounds (LMCs) used herein were coniferyl alcohol (CA), fractionated lignin from spruce wood (*Picea abies*) (FL-G) and maize stalks (*Zea mays L.*) (FL-GS), synthetic lignins (DHP-G) and commercial dimer (guaiacylglycerol-β-guaiacyl ether, G2).

CA was synthetized by reducing coniferyl aldehyde as described by Ludley *et al*[41]. FL-G and FL-GS were obtained by mild acidolysis in a dioxane/water (9/1, v/v) mixture[19]. DHP-G was prepared by peroxidase/hydrogen peroxide-mediated polymerization of CA, as detailed in a previous work[42]. The apparent weight-average molecular weight (Mw) and the number-average molecular weight (Mn) values for FL-GS, FL-G and DHP-G were assessed by size-exclusion chromatography and are summarized in the supplementary information (Table S1).

Guaiacylglycerol-β-guaiacyl ether was purchased from Tokyo Chemical Industry (Belgium). Iron(II) sulfate heptahydrate ($FeSO_4.7H_2O$, ACS reagent ≥ 99%), hydrogen peroxide ($H_2O_2$, 35 wt. % in $H_2O$), sulfuric acid ($H_2SO_4$, analytical purity), tetrahydrofuran (THF, analytical purity), toluene (analytical purity), methanol (analytical purity), 2,2-di(4-*tert*-octylphenyl)-1-picrylhydrazyl, and free radical (DPPH°) were purchased from Sigma Aldrich, France. DMSO-d6 (≥ 99.8%) and pyridine-d5 (≥ 99.5%) were purchased from Eurisotop, France.

**Film preparation:** Films were prepared from mixtures of cellulose nanocrystals (CNCs) and LMC by subjecting them to Fenton's reagent (0.16 mM $FeSO_4$, 1.6 mM $H_2O_2$). The initial mass of LMC represented 16.7% ($m_{LMC}/m_{film}$) of the total dry matter in the films prepared with Fenton's reagent and 16.3% of the total dry matter of the films prepared without Fenton's reagent. The measured pH of the suspensions was 4. In the optimal Fenton conditions, the pH of the suspensions was adjusted to 3 with 0.18 M sulfuric acid. All reactants were mixed by

magnetically stirring for 2 h at 40°C. This colloidal suspension remained stable throughout the Fenton reaction time. For casting, the total mixture (7.5 mL) was poured into a Teflon cylindrical cuvette and dried overnight under air at room temperature. All the films were named according to the following rules: $_{F}$[LMC-CNC]$^{pH}$ with F indicating that Fenton's reagent was used, pH indicating the adjusted pH of the suspension (3 or 4) and LMC indicating the type of starting material (CA, G2, FL-G, FL-GS, and DHP-G). When F was omitted, [LMC-CNC]$^{pH}$, the mixture did not undergo a Fenton reaction.

**Surface topography and nanomechanical measurements by atomic force microscopy (AFM):** AFM measurements were conducted on a Multimode 8 AFM (Bruker, USA) with 9.10 Nanoscope Software. All measurements were performed at 20°C and at a relative humidity of 45% in air by controlling the atmosphere in the sealed chamber around the AFM head with a Wetsys system (Setaram Instrumentation, France) for 4 h prior to any measurements with a humidity sensor data logger (Tinytag TV-4500) placed inside the chamber, as previously described[43]. All images were acquired at scan rates between 0.4 Hz and 0.9 Hz and with a resolution of 512*512 pixels. The topographical measurements were performed in PeakForce tapping mode (PFT) using Scan Asyst air probes (Bruker probes, USA) with a nominal resonance frequency of 70 kHz and a nominal spring constant of 0.4 N/m. The indentation modulus, E*, of the different samples was determined using the PeakForce Quantitative Nanomechanical property Mapping mode (PF-QNM). The measurements were performed with AFM TAP525 probes (Bruker probes, USA) with a nominal spring constant of 200 N/m and a nominal resonance frequency of 525 kHz. The high nominal spring constant of 200 N/m was consistent with the previously reported indentation modulus for similar films, which were on the order of a few GPa[30]. The tip radius was obtained by scanning a sharp-edge titanium roughness sample (model RS-15M, Bruker Probes, USA) before and after the experiments. Since the spring constant of the cantilevers was greater than 1 N/m, the Sader method was used

to evaluate the real spring constant[44]. The vertical AFM probe oscillation frequency was 2 kHz. After acquiring the data, force curves were collected on the mapping images, and the indentation moduli, $E^*$, which is more accurate regarding the anisotropic composition of cellulose[45], were calculated by fitting the linear region of the retracted part of the force curves using the Derjaguin-Muller-Toporov (DMT) model[30, 46] to take into account the adhesion forces, which are not negligible, and to consider the sharp AFM tip (radius less than 40 nm).[30, 43] For each indentation modulus value, at least 3 different areas of 3 similar samples were investigated. The values presented correspond to an average of 12,000 force curves acquired for the different samples.

**Hygroscopic properties by dynamic vapor sorption (DVS)**: A gravimetric sorption analyzer (IGA, Intelligent Gravimetric Analyzer, Hiden Isochema Ltd.) was used to determine the water sorption isotherm as described previously[29]. The experiment was performed at 20°C, and the relative humidity (RH) values ranged from 10 to 90%. The film (5 to 6 mg) was hydrated in steps of 10% RH during the water sorption phase and in 15% RH during desorption. The mass was recorded throughout the process until equilibrium was reached. All samples were dried by heating at 40°C under a flow of dry nitrogen for 240 min followed by cooling at 20°C under a flow of dry nitrogen for 480 min. The moisture content (MC) was calculated according to equation 5, where $m_{eq}$ is the mass of the sample in the equilibrium state and $m_d$ is the mass of the dry sample, measured after the drying sequence.

$$MC = \frac{m_{eq} - m_d}{m_d} \quad (1)$$

The sorption isotherms were adjusted with the PARK model (SI, experimental section) as previously published[29].

**Determination of molecular size**

Films were dissolved for 10 h in THF/toluene (95/5, v/v; 5 mg.mL$^{-1}$), and then the suspensions were filtered through a 0.45 µm PTFE membrane. The Mwvalues of the extracted fractions were estimated *via* high-performance size-exclusion chromatography (HPSEC) using a styrene-divinylbenzene PL-gel column (Polymer Laboratories, 5 µm, 100 Å, 600 mm x 7.5 mm I.D.) with THF/toluene (95/5, v/v; 1 mL.min$^{-1}$) as the eluent. The products were detected with a photodiode array device (Dionex Ultimate 3000 UV/vis detector) set at 280 nm. Toluene was used as an internal standard. Polymerization degrees were assessed from the apparent molar masses determined relative to a calibration curve based on polyethylene oxide standards (Igepal, Aldrich) and CA monomer and dimers.

**Chemical analysis**

**Fourier transform infrared (FTIR) spectroscopy:** Spectra were recorded on films using a Nicolet 6700 spectrophotometer. The tablets were prepared by mixing 200 mg of spectroscopic grade KBr with 3 mg of film. Spectra were recorded using 16 scans at a resolution of 4 cm$^{-1}$ from 800 to 4000 cm$^{-1}$ after background subtraction. The FTIR spectra were baseline corrected and normalized using the area of the spectra from 1900 to 800 cm$^{-1}$.

**Mass spectrometry:** Films were dissolved for 10 h in methanol (5 mg mL$^{-1}$). The resulting suspension was ultrafiltered (0.45 µm, GHP Acrodisc, Gelman). The recovered solution was injected (1 µL) for analysis by UHPLC (Thermo Fisher Scientific, Waltham, USA) with electrospray ionization mass spectrometry (ESI)-MS using a photodiode array (PDA) detector. Chromatography was performed using a C18 column (Highpurity, Thermo Electron Corporation, 2.7 µm, 50 mm x 2 mm I.D., Millipore). The elution gradient consisted of 5 to 100 vol. % aqueous acetonitrile and 1‰ HCOOH in 30 min at a flow rate of 0.4 mL.min$^{-1}$. ESI-MS spectra (120–2000 m/z) were acquired in negative mode using a quadrupole-time of flight (Q-

TOF) spectrometer (Impact II, Bruker) with a needle voltage of 4 kV and a desolvating capillary temperature of 350°C. The mass of the deprotonated ions and the fragmentation patterns were determined using the theoretical masses expected from the different types of CA oligomers[47].

**Nuclear magnetic resonance (NMR) spectroscopy:** Small pieces of the films were suspended in DMSO-d6/pyridine-d5 (4/1, v/v) by mechanical agitation (approximately 60 $mg.mL^{-1}$) before introduction into 5-mm NMR tubes. NMR spectra were recorded using a Bruker 600 MHz spectrometer with a TCI cryoprobe. HSQC experiments (Bruker standard pulse sequence "hsqcedetgpsisp.2.2") were carried out using the following parameters: nonuniform sampling 45%; 1874 points were acquired in F2 ($^{1}H$) with 32 scans, spectral width of 7211.539 Hz, and a relaxation delay of 1 s at 300 K; the F1 ($^{13}C$) dimension, with a spectral width of 24 751.277 Hz, was recorded with 386 time increments. Data processing was performed using Bruker's standard TopSpin-NMR 3.1 software. All spectra were manually phase corrected and calibrated to DMSO-d6 ($\delta_H$: 2.50 ppm, $\delta_C$: 39.5 ppm) as an internal standard. Spectral assignments were performed according to literature data[48, 49].

**Electron paramagnetic resonance (EPR) spectroscopy:** EPR spectra were recorded at 20°C using a Bruker 540 EPR spectrometer operating in the X band (9.85 GHz) under the following conditions: modulation frequency, 100 kHz; modulation amplitude, 10 G; time constant, 327.6 ms; conversion time, 327.91 ms; and microwave power, 10 mW. Data acquisition, processing, and double integration were performed using Bruker software. Approximately 20 mg of crushed film was added to the EPR tubes for analysis (Wilmad, 707-SQ-100M). The amplitude of the signal was calculated based on the difference between the maximum and the minimum of the spectra, which was possible because the EPR signal was symmetric.

To calculate the g factor of the film, a tube with DPPH° was analyzed under the same parameters to determine the magnetic field of DPPH under the experimental parameters ($B_{exp,DPPH°}$) and the theoretical magnetic field of DPPH° ($B_{th,DPPH°}$):

$$B_{th,DPPH} = \frac{\hbar \upsilon_{DPPH°}}{\beta g_{DPPH°}} \quad (2)$$

where ħ is Planck's constant (6.62 x $10^{-34}$ J.s), $\upsilon_{DPPH°}$ is frequency (Hz), β is the Bohr magneton (9.27 x $10^{-24}$ J.$T^{-1}$), and $g_{DPPH}$=2.0024.

The g factor of film, $g_{film,}$ was equal to

$$g_{film} = \frac{\hbar \upsilon_{film}}{\beta B_{corr}} \quad (3)$$

where $B_{corr} = B_{film} + (B_{th,\,DPPH°} - B_{exp,DPPH°})$ (4)

**Determination of the antioxidant properties by DPPH° tests:**

The free radical scavenging activities of phenols in solution and the cellulose films were evaluated by measuring their reactivities towards the stable free radical DPPH° according to a published method[17, 50].

In a quartz cuvette, 0.01 to 0.5 mg of square film pieces was added to 3 mL of a 6 × $10^{-5}$ mol.$L^{-1}$ DPPH˚ solution, which was prepared daily in absolute ethanol. The absorbance of each sample at 515 nm was monitored using a UV−visible double-beam spectrophotometer (Shimadzu Scientific Instrument UV-2401PC) until the absorbance plateaued. A blank was prepared under the same conditions without the film. In parallel, the free radical scavenging activity of LMC in solution was measured following a similar procedure. These measurements were made by combining 77 µL of LMC solution (from 0.1 to 1.25 mg.$mL^{-1}$) with 3 mL of 6 × $10^{-5}$ mol.$L^{-1}$ DPPH˚ solution, which was prepared daily in ethanol. A blank was prepared under the same conditions without the LMC sample solution.

All kinetics were obtained from at least five different concentrations or film masses in the concentration ranges described above by calculating the difference between the absorbance of the blank solution and the absorbance of the sample after 5 and 10 min. The percentage of residual DPPH° was calculated and plotted *vs* the concentration or the mass of LMC initially used in the sample. The effective concentration needed to reduce the initial DPPH° by 50% was determined from the corresponding curve and is expressed in $g_{LMC,initial}/g_{DPPH°}$.

**Results and discussion**

In this work, a new strategy to prepare CNC films containing lignin oligomers was explored. The properties of the resulting materials were characterized to evaluate the impact of the lignin on the structures at different observation scales. The strategy developed consisted of reacting CA with Fenton's reagent within a stable colloidal suspension of CNC to ideally achieve simultaneous grafting and polymerization to condense the film. The structure of the formed products along with the ultrastructure and physicochemical properties of the films were investigated.

The Fenton conditions were fixed and the same for all samples, and two pH values were used: pH 4, which is the pH of the prepared suspension of CNC, and pH 3, which corresponds to the optimal pH of the Fenton reaction[51]. In the first round of studies, the topographical, nanomechanical and water sorption properties of these materials were assessed, and the results were compared with respect to those previously published but obtained under different conditions[18, 19, 29, 30, 40]. In the second round of reactions, the antioxidant properties and radical stabilities of the films were investigated to tentatively establish the relationships between the structures of the chemical compounds formed, their organization within the film and the resulting properties of the obtained nanocomposites.

**Water sorption and nanomechanical properties of the CA-CNC films.**

The topographical, nanomechanical and water sorption properties were investigated by AFM and DVS. These analyses were performed on nanocellulose films made with Fenton's reagent in the presence of coniferyl alcohol at pH 3 and pH 4. To elucidate the reactivity of Fenton's reagent on CA, its fate, and its impact on the structure and properties of the corresponding films, two types of control materials were prepared in parallel. The first control was a film prepared with CA and CNC in the absence of Fenton's reagent (the $Fe^{2+}$ and $H_2O_2$ solutions were replaced with the same amounts of water) at pH 3 and 4 (Figure 1A; sample [CA-CNC]$^3$ and [CA-CNC]$^4$). The second control was a film prepared only from CNC in the presence (Figure 1A; samples $_F$[CNC]$^3$ and $_F$[CNC]$^4$) or absence of Fenton's reagent (Figure 1A, samples [CNC]$^3$ and [CNC]$^4$).

At the macroscale, all the control films were similarly transparent and brittle. The films prepared from CA, CNC and Fenton's reagent were also all transparent but showed different colors (light pink at pH 3 and colorless at pH 4). Moreover, they were mechanically resistant and easier to handle (Figure 1B). Observations of the films at the nanoscale indicated topographical variations. The films composed of CNCs with or without Fenton's reagent (Figure 1A, [CNC]$^{3or4}$ and $_F$[CNC]$^{3or4}$) showed disordered CNC rods (arrow). The presence of CA seemed to promote the alignment of the CNC rods in a more ordered manner (Figure 1A, [CA-CNC]$^4$). In contrast to the films prepared at pH 4, only a few nodules were observed in the films prepared at pH 3 both with and without Fenton's reagent (Figure 1A, [CA-CNC]$^3$ and $_F$[CA-CNC]$^3$, arrow). These nodules have previously been observed in films composed of CNC and isolated lignins or DHP-G regardless of the use of Fenton's reagent[18, 19], and the nodules were attributed to lignin oligomer aggregation. Thus, the presence of nodules in the film prepared at pH 3 suggested a different and stronger polymerization and/or aggregation process of CA at pH 3 than at pH 4, even without Fenton's reagent, leading to less homogeneous film

surfaces. These results demonstrate that the polymerization of CA was controlled by both pH and the Fenton reaction.

The indentation moduli of the films were calculated from their AFM images acquired in PF-QNM mode. The CNC and CA-CNC films obtained at pH 3 and 4 without Fenton's reagent showed similar indentation moduli, in the range of 10 GPa (Figure 2A, $[CNC]^4$, $[CNC]^3$, $[CA-CNC]^4$, and $[CA-CNC]^3$), which is consistent with previous measurements[30]. This result suggests that the influence of CA on the indentation modulus is not significant when the films are prepared without Fenton's reagent. In contrast, the combined presence of CA and Fenton's reagent was shown to increase the indentation moduli of the CNC films. Indeed, whereas Fenton's reagent increased the indentation moduli by 23% in the case of $_F[CNC]^4$ and 36% in the cases of $_F[CNC]^3$ and $_F[CA-CNC]^4$, the indentation modulus was increased by 85% for the $_F[CA-CNC]^3$ film (Figure 2A). These observations demonstrate that the combined contributions of the Fenton reactions of CNC and CA are essential to improve the mechanical properties at the nanoscale. This positive effect was exacerbated at pH 3 and could be due to both the oligomerization of CA and the interactions between CA oligomers and the cellulose nanorods during film preparation.

To complement these results, the water sorption isotherms of the CNC and CA-CNC films prepared at pH 3 and 4 were measured. All samples exhibited sigmoidal curves during water sorption and desorption in the 10-90% RH range (Figure 2B). The moisture contents (MC % values) of the CNC films prepared without or with Fenton's reagent at pH 3 or 4 ($[CNC]^3$, $_F[CNC]^3$, $[CNC]^4$ and $_F[CNC]^4$ films) were higher than those of films with CA ($[CA-CNC]^4$, $_F[CA-CNC]^4$, $[CA-CNC]^3$, and $_F[CA-CNC]^3$ films). The contents reached approximately 25% and 20% at 90% RH for CNC films without Fenton's reagent at pH 3 and 4, respectively, compared to approximately 20% and 18% at 90% RH for films containing CA. At pH 4, this difference was more pronounced in all RH ranges, with a maximum water content of 14% at

90% RH for $_F$[CA-CNC]$^4$ films prepared with Fenton's reagent, and the hysteresis between the sorption and desorption curves was less remarkable than that of the $_F$[CA-CNC]$^3$ films. The decrease in the water sorption of CNC films in the presence of CA is consistent with the hydrophobicity of CA oligomers and with literature related to the effects of phenolic compounds in cellulose-based materials[29, 52]. In addition to the intrinsic hydrophobicity of phenolic compounds, their distribution and organization in the film could also explain the water sorption reduction through barrier effects preventing water penetration into the cellulosic network. The effect was more pronounced when the films were prepared at pH 4, indicating that either the CNC or the polymerized CA was sensitive to the environment created by the $SO_3^-$-substituted cellulose, impacting the final structure and organization of the phenolic groups. This result was in agreement with topographic observations and permitted us to draw a schematic representation of the film (Figure 2C).

Indeed, the films made of CA, CNC and Fenton's reagent at pH 4 showed a more homogeneous distribution of CA on CNC relative to that of the films prepared at pH 3, which showed numerous nodules and aggregates (Figure 1A [CA-CNC]$^3$ and $_F$[CA-CNC]$^3$ films relative to [CA-CNC]$^4$ and $_F$[CA-CNC]$^4$ films). The intramolecular voids left between the assumed hydrophobic nodules form cavities where water molecules can access the CNC rods and become trapped, which could explain the higher water sorption at pH 3 than at pH 4.

To further clarify this difference, the film behaviors were compared using the PARK model to fit the water sorption isotherms (Figure S1). This analysis allowed us to distinguish 3 sorption mechanisms from the curves: the formation of water sorption sites on the surface of the molecules (represented by the $A_L$ parameters between 0 and 20% RH), the linear sorption of water molecules following Henry's law ($K_H$ parameters between 20 and 60% RH) and the formation of water molecule aggregates represented by $K_A$ and n (see the SI experimental session). All PARK parameter values indicated that the hygroscopicities of the CA-CNC films

were dependent on the pH during the Fenton reaction (Figure S1) and were consistent with the presence of water-trapping cavities in all CA-containing films formed at pH 3; Ka was higher for films prepared at pH 3 (0.224 ± 0.003 g/g dry matter) than it was for those obtained at pH 4 (0.157 ± 0.003 g/g dry matter) with respective n values of 8.0 ± 0.1 and 7.3 ± 0.2. The $A_L$ and $K_H$ values, corresponding to the formation of a uniform water layer, were lower for the $_F$[CA-CNC]$^4$ and [CA-CNC]$^4$ films than for the $_F$[CA-CNC]$^3$ and [CA-CNC]$^3$ films, confirming that the water layer on the surface of the CNC rods linked to CA units or oligomers was more uniform at pH 4 than at pH 3 (Figure S1). Moreover, the reactivity of Fenton's reagent with pure CNC seemed to be more greater at pH 3 than at pH 4, causing significant variations in the corresponding PARK parameters; $A_L$ increased (0.008 ± 0.001 to 0.013 ± 0.001 g/g dry matter), $K_H$ decreased (0.120 ± 0.003 to 0.091 ± 0.002 g/g dry matter) and finally Ka and n decreased (0.357 ± 0.009 to 0.220 ± 0.003 g/g dry matter with respective n values of 8.7 ± 0.2 and 7.8 ± 0.1). This observation suggests that in addition to the reactivity of the phenolic species, the chemical modification of the cellulose by the Fenton reaction contributes to the variations observed between nanocomposite films.

In conclusion, subjecting the components CA and CNC to the Fenton reaction before film formation increased the nanomechanical resistance and reduced the water sorption properties of the resulting films. These effects are dependent on the pH used during the film preparation. This can be explained by topographic differences in the formed material; namely, a continuous layer of phenolic moieties at pH 4 and nodules of phenolic moieties at pH 3 (Figure 2C). The interactions between the film components was strengthened by the oxidation of both CNC and the phenolics, and this change was more pronounced when the Fenton reaction was performed at pH 3. The generation of covalent or noncovalent bonds between CNC and CA is likely the basis of the good cohesion of the films. Additionally, we demonstrate that the simultaneous

presence of both Fenton's reagent and CA is mandatory to improve the water resistance of the formed films, confirming what was suggested formerly by Hambarzumyan *et al*.[18] (Figure S2).

Thus, the question of the covalent or noncovalent nature of the interactions generated by oxidative treatment has been addressed by investigating the chemical modifications and interactions that occurring during the CA-CNC mixed treatment and during film formation at the molecular scale.

**Chemical characterizations of the films**

**Entire films**. All films were analyzed by FTIR spectroscopy, and all the observed absorption bands were assigned based on the literature[53-56]. Characteristic bands of CNC and CA or their derivatives were observed at 1515 $cm^{-1}$ and 1603 $cm^{-1}$, corresponding to C=C bonds in aromatic molecules, and at 1060 $cm^{-1}$ and 1030 $cm^{-1}$, corresponding to OH groups in CNC (Figure 3). A new band at 1740 $cm^{-1}$ appeared in the spectra of all samples prepared in the presence of Fenton's reagent ($_F$[CNC]$^3$, $_F$[CNC]$^4$, $_F$[CA-CNC]$^3$, and $_F$[CA-CNC]$^4$). This band is consistent with the carbonyl band previously observed for CNC-DHP and CNC-lignin films by Hambardzumyan *et al.* (2015)[18] and was attributed to CNC oxidation products. The HSQC-NMR spectrum of the $_F$[CNC]$^4$ film dissolved in DMSO-d6/pyridine-d5 (4/1; v/v) showed a correlation between the signals at 110 ppm and 4.7 ppm (Figure 4), which was also observed in the spectra of the $_F$[CA-CNC]$^4$, $_F$[CA-CNC]$^3$ and $_F$[CNC]$^3$ films (data not shown). This correlation is characteristic of C1 of glucose. The appearance of such a signal could also indicate the depolymerization of cellulose by cleavage of the β-1-4 bonds and repolymerization into α-1-4 bonds, as suggested by Jérôme *et al.*[57]. These data are in agreement with the oxidation suggested by infrared analysis of the CNC films and demonstrate that the Fenton reaction can modify CNC at pH 3 and 4, probably through hydroxyl radicals inducing cleavage of the glycosidic bonds (β-1-4) to form the C1 carbonyl derivative of glucose[58] or by

isomerization of the β-1-4 bond to an α-1-4 bond[57]. Moreover, the HSQC-NMR spectra of CA-CNC films showed correlations among the β-O-4, β-β and β-5 structures, which confirmed the oligomerization of CA (data not shown). Nevertheless, it was not possible to calculate the proportion of these structures because of the excess CNC present in the films.

**Extracted compounds and film residues.**

We have shown that CA oxidation is essential for the formation of films with good cohesion properties. Thus, to assess the degree of polymerization of the compounds included in the CNC material during the Fenton reaction, the phenolic molecules extractable from films by a THF/toluene mixture were analyzed. Unfortunately, the components that strongly interact with CNC cannot be specifically analyzed.

The mass yield of the extract varied from 9 to 16% of the total dry matter of the film, depending on the composition of starting materials and the pH used for film preparation (Table 1). The recovered mass represented 58 to 99% of the initial mass of CA in the reaction mixture. This demonstrates that, depending on the presence of the Fenton's reagent and the pH, a significant fraction of the oligomers can strongly interact with the surface of the CNC. Furthermore, the experiments with CA and Fenton's reagent without CNC show that the products recovered in the extract represented 99 % of the initial mass of CA. That means the mineralization of CA by Fenton's reagent, sometimes described as an end–point of the reaction, can be overlooked in the experimental conditions[59] (Table 1).

The extractable CA oligomers were then subjected to size-exclusion chromatography (SEC). The analysis showed that in samples where Fenton's reagent was absent, a small amount of CA oligomerization occurred spontaneously at pH 4. This oligomerization was even more pronounced at pH 3. This highlighted the pH-dependence of the self-oxidation of CA, confirming previous reports[60, 61]. However, the underlying mechanism remains unclear,

although the involvement of ROS, trace elements, and radical formation on CA has been suggested.

When Fenton's reagent is used during film preparation, the extracted fractions had very different in molecular mass distributions. Indeed, in the extracted fractions of the films obtained at pH 4 (Figure 5A), oligomers with DP ≥ 3 were observed and represented approximately 50% of the total eluted structures (Figure 5B).

For films obtained at pH 3, including one treated with Fenton's reagent ($_F$[CA-CNC]$^3$), the elution profile is very similar to that of self-oxidized CA. However, 40% of the CA remained unextracted because it was strongly associated with CNC. However, the self-oxidation of CA, in the absence of Fenton's reagent, is not a side effect, as 25% of the material also remain within CNC film residu (sample [CA-CNC]$^3$, Table 1). It is then possible that the two phenomena occurred simultaneously in $_F$[CA-CNC]$^3$, leading to the particular features reported above (lignin nodules, water sorption and nanomechanical properties). In both cases, ($_F$[CA-CNC]$^3$ and [CA-CNC]$^3$), oligomers with DP ≥ 3 represented approximately 70% of the analyzed molecular populations. Moreover, the SEC profiles revealed some qualitative changes in the dimer composition, as indicated by the differences in the elution profiles between retention times of 15 and 16.5 min.

To identify the differences in the dimer structures, the methanol extracts of the films were analyzed by LC-MS (Table S2, Figure S3). The analysis showed that the dimer populations were more diverse in $_F$[CA-CNC]$^{3 \text{ or } 4}$ and included β-O-4 ([M-H] 375 g.mol$^{-1}$), β-5 ([M-H] 357 g.mol$^{-1}$) and β–β ([M-H] 357 g.mol$^{-1}$) dimers. A particular dimer, laricinol, L ([M-H] 359 g.mol$^{-1}$) was found in $_F$[CA-CNC]$^4$ film extracts; moreover, β-O-4, β-5 and β–β dimers were identified in the extracts of $_F$[CA-CNC]$^3$ films. In the absence of Fenton's reagent, no β-O-4 dimer was found and neither were β–β nor L dimers ([CA-CNC]$^3$ and [CA-CNC]$^4$ films). This

confirmed that CA underwent covalent coupling and that the oligomerization mechanism was influenced by the presence of Fenton's reagent.

As stated above, a significant fraction of CA and its oxidized products remain attached to the CNCs by covalent or strong interactions with the cellulose crystals. Thus, FTIR spectroscopy was performed on the extracted films to obtain a global overview of the compounds remaining on the nanostructured material.

The analysis of the film residues confirmed the presence of phenolic compounds associated with the CNCs in the films prepared with CA regardless of the pH used. Indeed, whereas the spectra of all the films exhibited characteristic bands of cellulose, such as C-H at 1282 $cm^{-1}$, C-O-C at 1165 and 900 $cm^{-1}$ and OH at 1206, 1060 and 1030 $cm^{-1}$ (Figure 6), the spectra of the ${}_{F}[CA\text{-}CNC]^{3}$ and ${}_{F}[CA\text{-}CNC]^{4}$ film residues showed an additional band at 1515 $cm^{-1}$, characteristic of C=C bonds of aromatic structures. Moreover, the presence of a band at 1740 $cm^{-1}$, assigned to carbonyl functions, was present in the spectra of CNC and CA-CNC films prepared with Fenton's reagent, indicating the presence of oxidized species in the CNC fractions of the films (see also the FTIR spectra of the whole films, above in the text).

This molecular investigation showed that CA oligomerization in the films prepared in the presence of Fenton's reagent could proceed via two mechanisms: self-oxidation and radical couplings induced by oxidation through Fenton's reagent. However, self-oxidation does not form the structures necessary for film cohesion. The Fenton reaction on either CNC or CA is mandatory to achieve properties suitable for packaging applications (transparency and hydrophobicity, sufficient water resistance, improved mechanical properties and antioxidant capacity). This does not preclude that self-oxidation can impact the final properties, but this point remains unclear. Indeed, the CA self-oxidation structures may also be oxidized by the Fenton reaction, contributing to film cohesion and the obtained properties. Despite the evidence

that the Fenton reaction impacted both the CNC and CA structures, no covalent bonds between the carbohydrates and phenolic compounds were detected by NMR spectroscopy. Additionally, no CA-glucose complexes could be identified by SEC or LC-MS.

A potential application of nanostructured materials, including lignins, is active packaging. We have reported here that the water and moisture content is dependent on the nanostructure of the material. Another property relevant to packaging applications[17, 62, 63] is the potential radical scavenging properties[64-66] of films due to the presence of CA and oligomers.

The relationships between the structural features of the films and the antioxidant properties and the presence of stable radicals in the material were then investigated.

**Antioxidant properties.**

To assess the impact of the film preparation on the antioxidant properties of CA, DPPH° tests were performed first on CA in solution and then on CA-CNC films prepared with Fenton's reagent. DPPH° is a stable free radical that can be reduced to DPPH-H by the phenolic moieties of an antioxidant molecule. The antioxidant activity of CA was evaluated by measuring the concentration needed to reduce 50% of the DPPH° (EC50), and this value was determined for the solution ($EC50_{sol}$) and for the films ($EC50_{film}$). The EC50 values measured in $g_{CAinitial}.g_{DPPH°}^{-1}$ are inversely proportional to the antioxidant activity. The $EC50_{sol}$ of CA was equal to 0.25 ± 0.01 $g_{CAinitial}.g^{-1}_{DPPH°}$. The $EC50_{film}$ of $_F$[AC-CNC]$^4$ was 0.40 ± 0.02 and that of $_F$[AC-CNC]$^3$ $_{was}$ 0.50 ± 0.03 $g_{CAinitial}.g_{DPPH°}^{-1}$ (Figure 7A). This EC50 values of the films increased by 60% and 100%, respectively, indicating that the antioxidant activity of CA was lower when it was in a film than when it was in solution. This could be explained both by the lower accessibility of the CA fraction trapped in the film and by the lower activity of the CA in its oxidized oligomerized form. Indeed, the antioxidant properties of the lignin oligomers were previously shown to decrease with increasing molar mass[66]. This explanation is corroborated by the lower radical

scavenging capacity of the film prepared at pH 3 ($_F$[AC-CNC]$^3$), which corresponded to a more extensive oligomerization of CA compared to that formed at pH 4 ($_F$[AC-CNC]$^4$).

To assess the influence of the degree of CA oligomerization on the antioxidant properties of the films, LMC obtained either by lignin isolation or by controlled *in vitro* CA oligomerization was used for film production. The $EC50_{sol}$ values of the LMCs used varied from 0.44 $g_{LMCinitial}.g_{DPPH°}^{-1}$ for G2 (Mw= 320 g.mol.$^{-1}$) to 1.46 $g_{LMCinitial}.g_{DPPH°}^{-1}$ for DHP-G (Mw = 4496 g.mol$^{-1}$), which is consistent with the literature[17, 62, 66]. After incorporation into a film using Fenton's reagent at pH = 4 ($_F$[LMC-CNC] $^4$), the apparent EC50 of the different LMCs increased by factors of 2 to 15. This increase was higher for isolated lignin fractions (FL-G and FL-GS) and synthetic lignins (DHP-G) than for CA and its dimers. This could be explained by the lower accessibility of the higher molar mass oligomers to DPPH°, as they are trapped in the film, analogous to the complex structures obtained with the CA samples $_F$[CA-CNC] $^4$) (Figure 2C).

To further elucidate the radical scavenging capacity of the films, considering the simultaneous presence of extractable and strongly immobilized molecules in the cellulose crystal material, the formation and evolution of radicals in the films was investigated by EPR.

**Relationships between the antioxidant and organic radical stability properties in the LMC-CNC films: EPR study**

The Fenton reaction involves ROS, and in particular the formation of hydroxy radicals, which turn phenols into phenoxy radicals and promote subsequent radical coupling reactions between phenolic compounds. On the other hand, the antioxidant tests performed on LMC confirmed their capacities to trap radicals both in solution and in films, and it is demonstrated in the literature that stable phenoxy radicals can exist in isolated lignins[67]. Thus, the ROS radicals formed by Fenton's reagent and LMC coupling products should be in equilibrium, and phenoxy

radicals should play a central role in this balance. To elucidate their role in film forming and antioxidant properties, direct tracking was performed by EPR analysis.

The films made without Fenton's reagent, [CA-CNC]$^3$ and [CA-CNC]$^4$, as well as those made with only CNC, did not show any EPR signals. In contrast, a clear signal was observed for films made with CA, CNCs and Fenton's reagent regardless of the pH ($_F$[CA-CNC]$^3$ and $_F$[CA-CNC]$^4$ films), confirming the presence of radicals in the material (Figure 7B). The g factor of the $_F$[CA-CNC]$^4$ film was calculated to be 2.0036. The g factor of the $_F$[CA-CNC]$^3$ film was 2.0030. These g values match those described in the literature for phenoxy radicals[68], and the difference in the measurements depends on the protonation of the radical[69].

The amplitude of the EPR signal was proportional to the mass of the film introduced in the EPR tube, which confirmed the homogeneous distribution of phenoxy radicals in the films. The amplitude of the phenoxy radical signal normalized to one gram of film was higher for films prepared at pH 4 than for those prepared at pH 3 (Figure 7B).

The comparison of the EPR data of different types of films showed that the oxidation of CA by Fenton's reagent was responsible for the formation of phenoxy radicals in the films. The most favorable conditions for the Fenton reaction, pH 3, led to a film containing fewer radicals. This suggests that the extent of the coupling reaction is more pronounced at pH 3 than at pH 4, a hypothesis consistent with the higher polymerization degrees and subsequent nodule formation observed at pH 3. Such nodules could concentrate the phenols/phenoxy components within a particular domain on the cellulose surface during the preparation of the films. The higher abundance of free radicals in the $_F$[CA-CNC]$^4$ film is related to the lower oligomerization degree of CA, suggesting a less complete reaction, compared to $_F$[CA-CNC]$^3$. Also, the absence of nodules in final material suggest that a more homogeneous immobilization of the coupling products on well aligned cellulose nanocrystals could favorize the stabilization of phenoxy radicals (Figure 1A). Finally, the measurements performed after storage of $_F$[CA-CNC]$^4$ and

$_F$[CA-CNC]$^3$ in the dark at a controlled temperature indicated that the phenoxy radicals remained persistent in the material for at least 3 months (17.70 ± 0.01) x $10^6$ u.$a_{amplitude}$.$g^{-1}$ and (10.07 ± 0.01) x $10^6$ u.$a_{amplitude}$.$g^{-1}$).

All the LMC-CNC films prepared with Fenton's reagent also exhibited a phenoxy radical signal with an amplitude depending on the LMC used. The measured signals, expressed per gram of film, are proportional to the LMC-$EC50_{sol}$ values (Figure 8) and thus are also proportional to the apparent average molar mass of the LMC. This result showed that the capacity of the LMC to be oxidized by Fenton's reagent during film preparation could be predicted by its capacity to be oxidized by DPPH° in solution, namely hydrogen abstraction from the LMC phenol. It also indicates that some of the phenoxy radicals formed did not undergo coupling and were immobilized in the matrix formed by the CNC and the nonradical end-products of the oxidations. Thus, we demonstrate here that it is possible to use the CNC-LMC-Fenton system to tune the production of stable phenoxy radicals in the composite material, which offers potential applications in the field of electrochemically active materials[70], such as probes and batteries[71].

## Conclusions

This study confirmed that the Fenton reaction on CNC and LMC was necessary to obtain a consolidated film with improved hydrophobicity and nanomechanical properties. Several effects of Fenton's reagent were observed at different scales, and the conversion of the hydroxyl groups of CNCs into carbonyls, the isomerization of CNC β 1-4 bonds, and the pH-dependent oligomerization of CA with the formation of nodules (observed specifically at pH 3) were tentatively attributed to these effects. All these effects showed that either the oxidation of CNCs and CA by Fenton's reagent and the self-oxidation of CA were essential for generating strong noncovalent interactions among the CNC-phenolics. In addition to their mechanical and water

resistance, the films showed lower antioxidant properties and capacity to trap and stabilize radicals, which could be modulated by both pH and the molar mass of the LMC used, probably through the different structural features formed between the CNCs and the oxidized phenols.

The possibility of persistent phenoxy radicals in film and the relationship between the quantity of these radicals and the antioxidant properties of LMC suggests potential applications, for instance, where stable organic radical polymers (ORPs) are needed.

**Supporting Information**. Weight-average (Mw) and number-average (Mn) molecular weights of the lignin model compounds (LMCs) (Table S1); Fitting results of water sorption isotherms by PARK model (Figure S1 and text); Water washing resistance of $_{F}$[CA-CNC]$^{pH}$ films (Figure S2); Chemical structures extracted from $_{F}$[CA-CNC]$^{pH}$ films and identified by LCMS (Table S2); UV-MS data on extracted fractions of $_{F}$[CA-CNC]$^{pH}$ and [CA-CNC]$^{pH}$ films (Figure S3); antioxidant properties of LMCs in ethanolic solution and in films (Figure S4).

**Corresponding Author**

*Veronique Aguié-Béghin - Email: veronique.aguie@inrae.fr

**Author Contributions**

The manuscript was written through contributions of all authors. All authors have given approval to the final version of the manuscript.

**Acknowledgments**

The authors thank platforms Nano'mat and Planet of University Reims-Champagne Ardennes and the IJPB Institute Plant Observatory Chemistry and Metabolism Platform as well as A. Habrant, (Fractionnement des AgroRessources et Environnement, UMR FARE A 614), A. Majira, C. Lapierre, F. Pion, L. Cezard, S. Boutet (Institut Jean-Pierre Bourgin , IJPB) for their

technical support and fruitful discussions. The IJPB research unit benefits from the support of the LabEx Saclay Plant Sciences-SPS (ANR-10-LABX-552 0040-SPS).

**Funding Sources**

This work was financially supported by the Agence Nationale de la Recherche (ANR) through the Carnot Institutes 3BCAR (www.3bcar.fr) and Qualiment (https://qualiment.fr/) as well as by INRAE resources, under the Lignoxyl 1&2 projects, in accordance with amendment No. 3 No. 19-CARN-001-01 to financial support agreement No. 16-CARN 0001-01N° and the Scientific Department, TRANSFORM of INRAE.

**Notes**

The authors declare no competing financial interest.

**Abbreviations**

AFM, atomic force microscopy; CA, coniferyl alcohol; CNC, cellulose nanocrystal; CNF, cellulose nanofibril; DHP, dehydropolymer; DHP-G: dehydropolymer of coniferyl alcohol; DMT, Derjaguin-Muller-Toporov model; DPPH°, 2,2′-diphenyl-1-picrylhydrazyl; DVS, dynamic vapor sorption; EPR, electron paramagnetic resonance; FL-G, fractionated lignin from spruce wood (*Picea abies*); FL-GS, fractionated lignin from maize stalks (*Zea mays L.*); FTIR, Fourier transform infrared; G2, guaiacylglycerol-β-guaiacyl ether; LMC, lignin model compound; MC, moisture content; NMR, nuclear magnetic resonance; ORPs, stable organic radical polymer; PF-QMN, PeakForce Quantitative Nanomechanical; PFT, PeakForce tapping mode; RH, relative humidity; ROS, reactive oxygen species; UHPLC, ultrahigh-performance liquid chromatography

REFERENCES

1. Eichhorn, S. J.; Dufresne, A.; Aranguren, M.; Marcovich, N. E.; Capadona, J. R.; Rowan, S. J.; Weder, C.; Thielemans, W.; Roman, M.; Renneckar, S.; Gindl, W.; Veigel, S.; Keckes, J.; Yano, H.; Abe, K.; Nogi, M.; Nakagaito, A. N.; Mangalam, A.; Simonsen, J.; Benight, A. S.; Bismarck, A.; Berglund, L. A.; Peijs, T., Review: current international research into cellulose nanofibres and nanocomposites. *J. Mater. Sci.* **2010,** 45 (1), 1-33.
2. Moon, R. J.; Martini, A.; Nairn, J.; Simonsen, J.; Youngblood, J., Cellulose nanomaterials review: structure, properties and nanocomposites. *Chem. Soc. Rev.* **2011,** 40 (7), 3941-3994.
3. Sharma, A.; Thakur, M.; Bhattacharya, M.; Mandal, T.; Goswami, S., Commercial application of cellulose nano-composites – A review. *Biotechnology Reports* **2019,** 21, e00316.
4. CelluForce, https://www.celluforce.com/en/about-celluforce/who-we-are/
5. Lavoine, N.; Desloges, I.; Dufresne, A.; Bras, J., Microfibrillated cellulose – Its barrier properties and applications in cellulosic materials: A review. *Carbohydr. Polym.* **2012,** 90 (2), 735-764.
6. Siqueira, G.; Bras, J.; Dufresne, A., Cellulosic bionanocomposites: a review of preparation, properties and applications. *Polymers* **2010,** 2 (4), 728-765.
7. Mu, X. Y.; Gray, D. G., Droplets of cellulose nanocrystal suspensions on drying give iridescent 3-D "coffee-stain" rings. *Cellulose* **2015,** 22 (2), 1103-1107.
8. Curvello, R.; Raghuwanshi, V. S.; Garnier, G., Engineering nanocellulose hydrogels for biomedical applications. *Adv.Colloid Interface Sci.* **2019,** 267, 47-61.
9. Rahmat, M.; Karrabi, M.; Ghasemi, I.; Zandi, M.; Azizi, H., Silane crosslinking of electrospun poly (lactic acid)/nanocrystalline cellulose bionanocomposite. *Mater. Sci. Eng. C* **2016,** 68, 397-405.
10. Sun, X.; Wu, Q.; Ren, S.; Lei, T., Comparison of highly transparent all-cellulose nanopaper prepared using sulfuric acid and TEMPO-mediated oxidation methods. *Cellulose* **2015,** 22 (2), 1123-1133.
11. Bajwa, D. S.; Pourhashem, G.; Ullah, A. H.; Bajwa, S. G., A concise review of current lignin production, applications, products and their environmental impact. *Ind. Crop. Prod.* **2019,** 139, 111526.
12. Sarkanen, K. V.; Ludwig, C. H., *Lignins: Occurrence, formation, structure and reactions*. Eds. John Wiley & Sons, Inc., New York, 1971; p 916.
13. Paone, E.; Tabanelli, T.; Mauriello, F., The rise of lignin biorefinery. *Curr. Opin. Green Sustain. Chem.* **2020,** 24, 1-6.
14. Gao, Y.; Qu, W.; Liu, Y.; Hu, H.; Cochran, E.; Bai, X., Agricultural residue-derived lignin as the filler of polylactic acid composites and the effect of lignin purity on the composite performance. *J. Appl. Polym. Sci.* **2019,** 136 (35), 47915.
15. Brodin, I.; Ernstsson, M.; Gellerstedt, G.; Sjöholm, E., Oxidative stabilisation of kraft lignin for carbon fibre production. *Holzforschung*, **2012**, 66, 141-147.
16. Norberg, I.; Nordström, Y.; Drougge, R.; Gellerstedt, G.; Sjöholm, E., A new method for stabilizing softwood kraft lignin fibers for carbon fiber production. *J. Appl. Polym. Sci.* **2013,** 128 (6), 3824-3830.
17. Aguié-Béghin, V.; Foulon, L.; Soto, P.; Crônier, D.; Corti, E.; Legée, F.; Cézard, L.; Chabbert, B.; Maillard, M.-N.; Huijgen, W. J. J.; Baumberger, S., Use of Food and Packaging Model Matrices to Investigate the Antioxidant Properties of Biorefinery Grass Lignins. *J. Agric. Food Chem.* **2015,** 63 (45), 10022-10031.

18. Hambardzumyan, A.; Foulon, L.; Bercu, N. B.; Pernes, M.; Maigret, J. E.; Molinari, M.; Chabbert, B.; Aguié-Béghin, V., Organosolv lignin as natural grafting additive to improve the water resistance of films using cellulose nanocrystals. *Chem. Eng. J.* **2015,** 264, 780-788.
19. Hambardzumyan, A.; Foulon, L.; Chabbert, B.; Aguié-Béghin, V., Natural Organic UV-Absorbent Coatings Based on Cellulose and Lignin: Designed Effects on Spectroscopic Properties. *Biomacromolecules* **2012,** 13 (12), 4081-4088.
20. Kloser, E.; Gray, D. G., Surface Grafting of Cellulose Nanocrystals with Poly(ethylene oxide) in Aqueous Media. *Langmuir* **2010,** 26 (16), 13450-13456.
21. Lizundia, E.; Meaurio, E.; Vilas, J., Chapter 3 - Grafting of Cellulose Nanocrystals. In *Multifunctional Polymeric Nanocomposites Based on Cellulosic Reinforcements*, Puglia, D.; Fortunati, E.; Kenny, J. M., Eds. William Andrew Publishing, 2016; p 61.
22. Prathapan, R.; Thapa, R.; Garnier, G.; Tabor, R. F., Modulating the zeta potential of cellulose nanocrystals using salts and surfactants. *Colloids Surf., A* **2016,** 509, 11-18.
23. Abitbol, T.; Kam, D.; Levi-Kalisman, Y.; Gray, D. G.; Shoseyov, O., Surface Charge Influence on the Phase Separation and Viscosity of Cellulose Nanocrystals. *Langmuir* **2018,** 34 (13), 3925-3933.
24. Eyley, S.; Thielemans, W., Surface modification of cellulose nanocrystals. *Nanoscale* **2014,** 6 (14), 7764-7779.
25. Zoppe, J. O.; Grosset, L.; Seppala, J., Liquid crystalline thermosets based on anisotropic phases of cellulose nanocrystals. *Cellulose* **2013,** 20 (5), 2569-2582.
26. Azzam, F.; Heux, L.; Jean, B., Adjustment of the Chiral Nematic Phase Properties of Cellulose Nanocrystals by Polymer Grafting. *Langmuir* **2016,** 32 (17), 4305-4312.
27. Sadeghifar, H.; Venditti, R.; Jur, J.; Gorga, R. E.; Pawlak, J. J., Cellulose-Lignin Biodegradable and Flexible UV Protection Film. *ACS Sustainable Chem. Eng.* **2017,** 5 (1), 625-631.
28. Kalashnikova, I.; Bizot, H.; Cathala, B.; Capron, I., Modulation of Cellulose Nanocrystals Amphiphilic Properties to Stabilize Oil/Water Interface. *Biomacromolecules* **2012,** 13 (1), 267-275.
29. Muraille, L.; Pernes, M.; Habrant, A.; Serimaa, R.; Molinari, M.; Aguié-Béghin, V.; Chabbert, B., Impact of lignin on water sorption properties of bioinspired self-assemblies of lignocellulosic polymers. *Eur.Polym. J.* **2015,** 64, 21-35.
30. Muraille, L.; Aguié-Beghin, V.; Chabbert, B.; Molinari, M., Bioinspired lignocellulosic films to understand the mechanical properties of lignified plant cell walls at nanoscale. *Sci. Rep.* **2017,** 7, 44065.
31. Contreras, D.; Freer, J.; Rodríguez, J., Veratryl alcohol degradation by a catechol-driven Fenton reaction as lignin oxidation by brown-rot fungi model. *Int. Biodeterior. Biodegrad.* **2006,** 57 (1), 63-68.
32. Gierer, J.; Reitberger, T., The Reactions of Hydroxyl Radicals with Aromatic Rings in Lignins, Studied with Creosol and 4-Methylveratrol. *Holzforschung* **1992**, 46 (6) 495-504.
33. Kent, M. S.; Zeng, J.; Rader, N.; Avina, I. C.; Simoes, C. T.; Brenden, C. K.; Busse, M. L.; Watt, J.; Giron, N. H.; Alam, T. M.; Allendorf, M. D.; Simmons, B. A.; Bell, N. S.; Sale, K. L., Efficient conversion of lignin into a water-soluble polymer by a chelator-mediated Fenton reaction: optimization of H2O2 use and performance as a dispersant. *Green Chem.* **2018,** 20 (13), 3024-3037.
34. Zazo, J. A.; Casas, J. A.; Mohedano, A. F.; Gilarranz, M. A.; Rodríguez, J. J., Chemical Pathway and Kinetics of Phenol Oxidation by Fenton's Reagent. *Environ. Sci.Technol.* **2005,** 39 (23), 9295-9302.

35. Areskogh, D.; Henriksson, G., Chemical Pulping: Fenton's reaction: a simple and versatile method to structurally modify commercial lignosulphonates. *Nord. Pulp Pap. Res. J.* **2011**, 26 (1), 90-98.
36. Zhao, X.; Yang, B.; Li, L.; Zhang, F.; Linhardt, R. J., On-line separation and characterization of hyaluronan oligosaccharides derived from radical depolymerization. *Carbohydr. Polym.* **2013,** 96 (2), 503-509.
37. Arantes, V.; Milagres, A. M. F., Degradation of cellulosic and hemicellulosic substrates using a chelator-mediated Fenton reaction. *J. Chem. Technol.Biotechnol.* **2006,** 81 (3), 413-419.
38. Dai, Y.; Shao, C.; Piao, Y.; Hu, H.; Lu, K.; Zhang, T.; Zhang, X.; Jia, S.; Wang, M.; Man, S., The mechanism for cleavage of three typical glucosidic bonds induced by hydroxyl free radical. *Carbohydr. Polym.* **2017,** 178, 34-40.
39. Wang, Z. X.; Li, G.; Yang, F.; Chen, Y. L.; Gao, P., Electro-Fenton degradation of cellulose using graphite/PTFE electrodes modified by 2-ethylanthraquinone. *Carbohydr. Polym.* **2011,** 86 (4), 1807-1813.
40. Hambardzumyan, A.; Molinari, M.; Dumelie, N.; Foulon, L.; Habrant, A.; Chabbert, B.; Aguié-Béghin, V., Structure and optical properties of plant cell wall bio-inspired materials: Cellulose-lignin multilayer nanocomposites. *C. R. Biol.* **2011,** 334 (11), 839-850.
41. Ludley, F. H.; Ralph, J., Improved preparation of coniferyl and sinapyl alcohols. *J. Agric. Food Chem.* **1996,** 44 (10), 2942-2943.
42. Cathala, B.; Saake, B.; Faix, O.; Monties, B., Evaluation of the reproducibility of the synthesis of dehydrogenation polymer models of lignin. *Polym. Degrad. Stab.* **1998,** 59 (1), 65-69.
43. Marcuello, C.; Foulon, L.; Chabbert, B.; Aguié-Béghin, V.; Molinari, M., Atomic force microscopy reveals how relative humidity impacts the Young's modulus of lignocellulosic polymers and their adhesion with cellulose nanocrystals at the nanoscale. *Int. J. Biol. Macromol.* **2020,** 147, 1064-1075.
44. Sader, J. E.; Chon, J. W. M.; Mulvaney, P., Calibration of rectangular atomic force microscope cantilevers. *Rev. Sci. Instrum.* **1999,** 70 (10), 3967-3969.
45. Cave, I. D., The anisotropic elasticity of the plant cell wall. *Wood Sci.Technol.* **1968,** 2 (4), 268-278.
46. Derjaguin, B. V.; Muller, V. M.; Toporov, Y. P., Effect of contact deformations on the adhesion of particles. *J. Colloid Interface Sci.* **1975,** 53 (2), 314-326.
47. Demont-Caulet, N.; Lapierre, C.; Jouanin, L.; Baumberger, S.; Mechin, V., Arabidopsis peroxidase-catalyzed copolymerization of coniferyl and sinapyl alcohols: Kinetics of an endwise process. *Phytochemistry* **2010,** 71 (14-15), 1673-1683.
48. Kim, H.; Ralph, J., Solution-state 2D NMR of ball-milled plant cell wall gels in DMSO-d6/pyridine-d5. *Org. Biomol. Chem.* **2010,** 8 (3), 576-591.
49. Kim, H.; Ralph, J., A gel-state 2D-NMR method for plant cell wall profiling and analysis: a model study with the amorphous cellulose and xylan from ball-milled cotton linters. *RSC Adv.* **2014,** 4 (15), 7549-7560.
50. Brand-Williams, W.; Cuvelier, M. E.; Berset, C., Use of a free radical method to evaluate antioxidant activity. *LWT - Food Sci.Technol.* **1995,** 28 (1), 25-30.
51. Litter, M. I.; Slodowicz, M., An overview on heterogeneous Fenton and photoFenton reactions using zerovalent iron materials. *J. Adv. Oxid. Technol.* **2017,** 20 (1), 19.
52. Notley, S. M.; Norgren, M., Surface Energy and Wettability of Spin-Coated Thin Films of Lignin Isolated from Wood. *Langmuir* **2010,** 26 (8), 5484-5490.

53. Gierlinger, N.; Goswami, L.; Schmidt, M.; Burgert, I.; Coutand, C.; Rogge, T.; Schwanninger, M., In Situ FT-IR Microscopic Study on Enzymatic Treatment of Poplar Wood Cross-Sections. *Biomacromolecules* **2008,** 9 (8), 2194-2201.
54. Kačuráková, M.; Capek, P.; Sasinková, V.; Wellner, N.; Ebringerová, A., FT-IR study of plant cell wall model compounds: pectic polysaccharides and hemicelluloses. *Carbohydr. Polym.* **2000,** 43 (2), 195-203.
55. Schwanninger, M.; Rodrigues, J. C.; Pereira, H.; Hinterstoisser, B., Effects of short-time vibratory ball milling on the shape of FT-IR spectra of wood and cellulose. *Vib. Spectrosc.* **2004,** 36 (1), 23-40.
56. Xu, F.; Yu, J.; Tesso, T.; Dowell, F.; Wang, D., Qualitative and quantitative analysis of lignocellulosic biomass using infrared techniques: A mini-review. *Appl. Energy* **2013,** 104, 801-809.
57. Jérôme, F.; Chatel, G.; De Oliveira Vigier, K., Depolymerization of cellulose to processable glucans by non-thermal technologies. *Green Chem.* **2016,** 18 (14), 3903-3913.
58. Kirk, T. K.; Ibach, R.; Mozuch Michael, D.; Conner Anthony, H.; Highley, L., Characteristics of Cotton Cellulose Depolymerized by a Brown-Rot Fungus, by Acid, or by Chemical Oxidants. *Holzforschung*, **1991**, 45 (4), 239-244.
59. Bach, A.; Shemer, H.; Semiat, R., Kinetics of phenol mineralization by Fenton-like oxidation. *Desalination* **2010,** 264, (3), 188-192.
60. Pomar, F.; Caballero, N.; Pedreño, M. a. A.; Ros Barceló, A., H2O2 generation during the auto-oxidation of coniferyl alcohol drives the oxidase activity of a highly conserved class III peroxidase involved in lignin biosynthesis. *FEBS Letters* **2002,** 529, (2), 198-202.
61. Uraki, Y.; Suzuki, K.; Ubukata, M., Polymerization of coniferyl alcohol by chain reaction. Another reaction for lignin formation. *Cellul. Chem.Technol.***2007,** 41, (9-10), 505-509.
62. Domenek, S.; Louaifi, A.; Guinault, A.; Baumberger, S., Potential of lignins as antioxidant additive in active biodegradable packaging materials. *J. Polym. Environ.* **2013,** 21 (3), 692-701.
63. Ge, Y.; Wei, Q.; Li, Z., Preparation and evaluation of the free radical scavenging activities of nanoscale lignin biomaterials. *BioResources* **2014,** 9, (4), 6699-6706.
64. Barclay, L. R. C.; Xi, F.; Norris, J. Q., Antioxidant properties of phenolic lignin model compounds. *J. Wood Chem.Technol.* **1997,** 17 (1-2), 73-90.
65. Dizhbite, T.; Telysheva, G.; Jurkjane, V.; Viesturs, U., Characterization of the radical scavenging activity of lignins—natural antioxidants. *Bioresour. Technol.* **2004,** 95 (3), 309-317.
66. Majira, A.; Godon, B.; Foulon, L.; van der Putten, J. C.; Cezard, L.; Thierry, M.; Pion, F.; Bado-Nilles, A.; Pandard, P.; Jayabalan, T.; Aguie-Beghin, V.; Ducrot, P. H.; Lapierre, C.; Marlair, G.; Gosselink, R. J. A.; Baumberger, S.; Cottyn, B., Enhancing the Antioxidant Activity of Technical Lignins by Combining Solvent Fractionation and Ionic-Liquid Treatment. *ChemSusChem* **2019,** 12, (21), 4799-4809.
67. Patil, S. V.; Argyropoulos, D. S., Stable Organic Radicals in Lignin: A Review. *ChemSusChem* **2017,** 10, (17), 3284-3303.
68. Park, J. S. B.; Wood, P. M.; Gilbert, B. C.; Whitwood, A. C., EPR Evidence for hydroxyl- and substrate-derived radicals in Fe(II)-oxalate/hydrogen peroxide reactions. The importance of the reduction of Fe(III)-oxalate by oxygen-conjugated radicals to regenerate Fe(II) in reactions of carbohydrates and model compounds. *Journal of the Chemical Society-Perkin Transactions 2* **1999**, (5), 923-931.
69. Sun, L.; Burkitt, M.; Tamm, M.; Raymond, M. K.; Abrahamsson, M.; LeGourriérec, D.; Frapart, Y.; Magnuson, A.; Kenéz, P. H.; Brandt, P.; Tran, A.; Hammarström, L.; Styring, S.;

Åkermark, B., Hydrogen-Bond Promoted Intramolecular Electron Transfer to Photogenerated Ru(III): A Functional Mimic of TyrosineZ and Histidine 190 in Photosystem II. *J. Am. Chem. Soc.* **1999,** 121 (29), 6834-6842.
70. Zhang, K.; Monteiro, M. J.; Jia, Z., Stable organic radical polymers: synthesis and applications. *Polym. Chem.* **2016,** 7 (36), 5589-5614.
71. Tenhaeff, W. E.; Rios, O.; More, K.; McGuire, M. A., Highly Robust Lithium Ion Battery Anodes from Lignin: An Abundant, Renewable, and Low-Cost Material. *Adv. Funct. Mater.* **2014,** 24, (1), 86-94.

FIGURE CAPTIONS

Figure 1: (A) Topographic images of $_F$[CNC]$^{pH}$ and $_F$[CA-CNC]$^{pH}$ films by AFM (size scan 10 µm x 10 µm, arrows show CNC rods or nodules of CA oligomers). (B) Photographs of the corresponding films prepared with Fenton's reagent.

Figure 2: (A) Indentation modulus measured by AFM at the nanoscale; (B) water sorption isotherms of $_F$[CNC]$^{pH}$ and $_F$[CA-CNC]$^{pH}$ films and (C) schematic of the hypothetical film structure at 45% RH ($_F$[CA-CNC]$^4$ and $_F$[CA-CNC]$^3$).

Figure 3: FTIR spectra of $_F$[CNC]$^{pH}$ and $_F$[CA-CNC]$^{pH}$ films. The vertical lines indicates the main bands of CNCs (gray) and CA oligomers (orange).

Figure 4: Anomeric region of the 2D $^{13}$C-$^1$H HSQC spectra of the CNC-based films solubilized in DMSO

Figure 5: (A) SEC profiles of the extracted fractions of $_F$[CA-CNC]$^{pH}$ films, (B) relative percentage of each type of CA oligomer (relative percentage = area of one identified chemical species divided by the sum of all areas of identified chemical species). Each specie V: vanillin, Ald: coniferyl aldehyde, FA: ferulic acid, T: toluene, DP: degree of polymerization was represented in A and B graphics in similar color index.

Figure 6: FTIR spectra of the residue of $_F$[CA-CNC]$^{pH}$ films. Vertical lines indicate the main bands of the CNCs (gray) and CA oligomers (orange).

Figure 7: (A) Antioxidant properties of CA in solution or in CNC-based films, (B) X band EPR spectra of crushed films $_F$[CA-CNC]$^{pH}$, g value of $_F$[CA-CNC]$^3$ = 2.0030 and $_F$[CA-CNC]$^4$ = 2.0036 (v = 9.82 x 109 Hz).

Figure 8: Relationship between the antioxidant properties of LMCs in solution and the phenoxy radical amplitude in the $_F$[LMC-CNC]$^4$ films. Insert X band EPR spectra of crushed films $_F$[LMC-CNC]$^4$, g value $_F$[CA-CNC]$^4$ = 2.0036 (v = 9.82 x 109 Hz).

Table 1: Mass yield of $_F$[CA-CNC]$^{pH}$ film and $_F$[CA]$^{pH}$ extractions by THF/toluene

| % (w/w) | $_F$[CA-CNC]$^4$ | [CA-CNC]$^4$ | $_F$[CA-CNC]$^3$ | [CA-CNC]$^3$ | $_F$[CA]$^{3or4}$ |
|---|---|---|---|---|---|
| $m_{CA}/ m_{film}$ | 16,7 | 16,3 | 16,7 | 16,3 | 95 |
| $MY_{ext/film} = \frac{m_{ext}}{m_{film}}$ | 12 | 16 | 9 | 13 | 99 |
| $MY_{ext/CA} = \frac{m_{ext}}{m_{CA}}$ | 73 | 99 | 58 | 73 | 100 |

MY: mass yield, $m_{CA}$: initial mass of CA, $m_{film}$ : mass of total dry film matter, $m_{ext}$: mass of dry extracted fraction

**For Table of Contents Graphic Use Only**

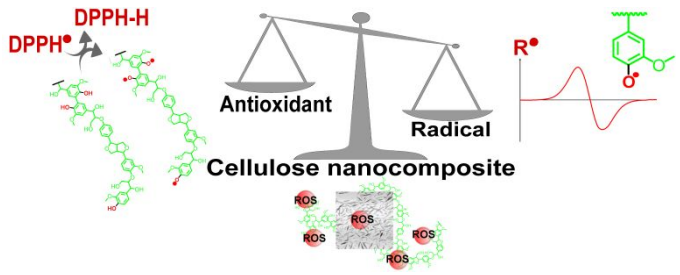


"Dual antioxidant properties and organic radical stabilization in cellulose nanocomposite films functionalized by polymerization of coniferyl alcohol"

*Elise Gerbin†,‡, Yves-Michel Frapart#, Carlos Marcuello†, Betty Cottyn‡, Laurence Foulon†, Miguel Pernes†, David Cronier†, Michael Molinari§, Brigitte Chabbert†, Paul-Henri Ducrot‡, Stéphanie Baumberger‡, Véronique Aguié-Béghin†*, Bernard Kurek†*

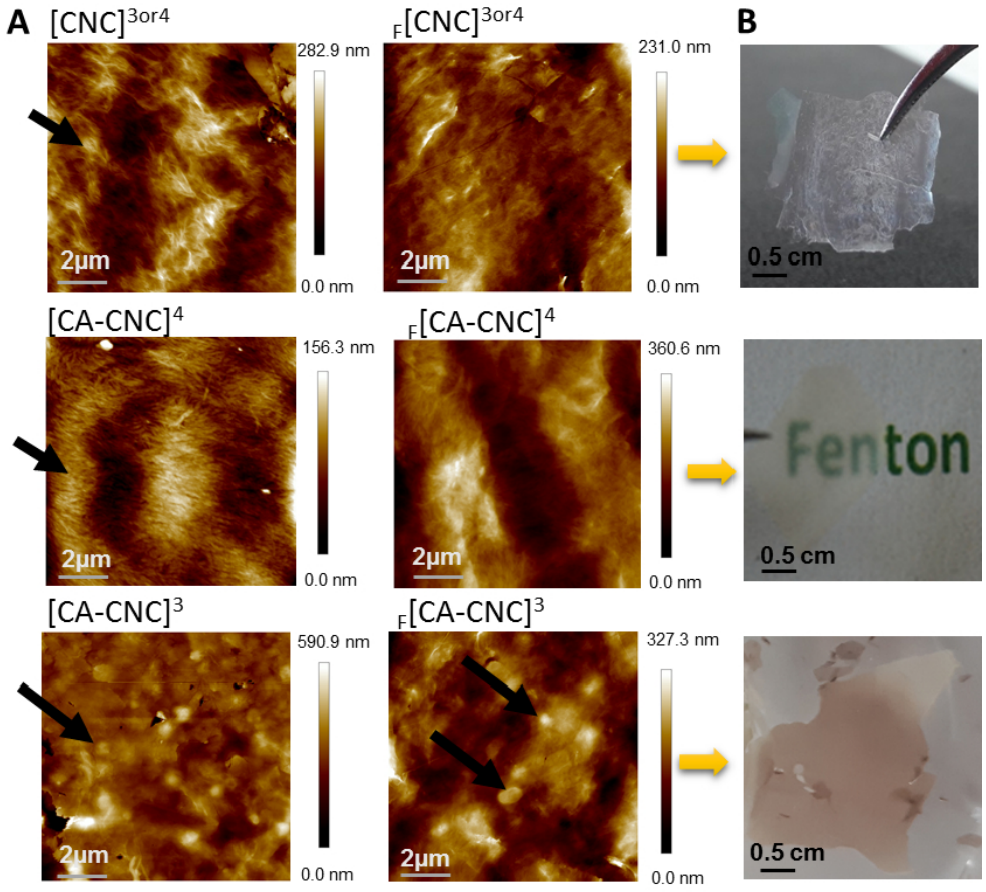


165x151mm (131 x 131 DPI)

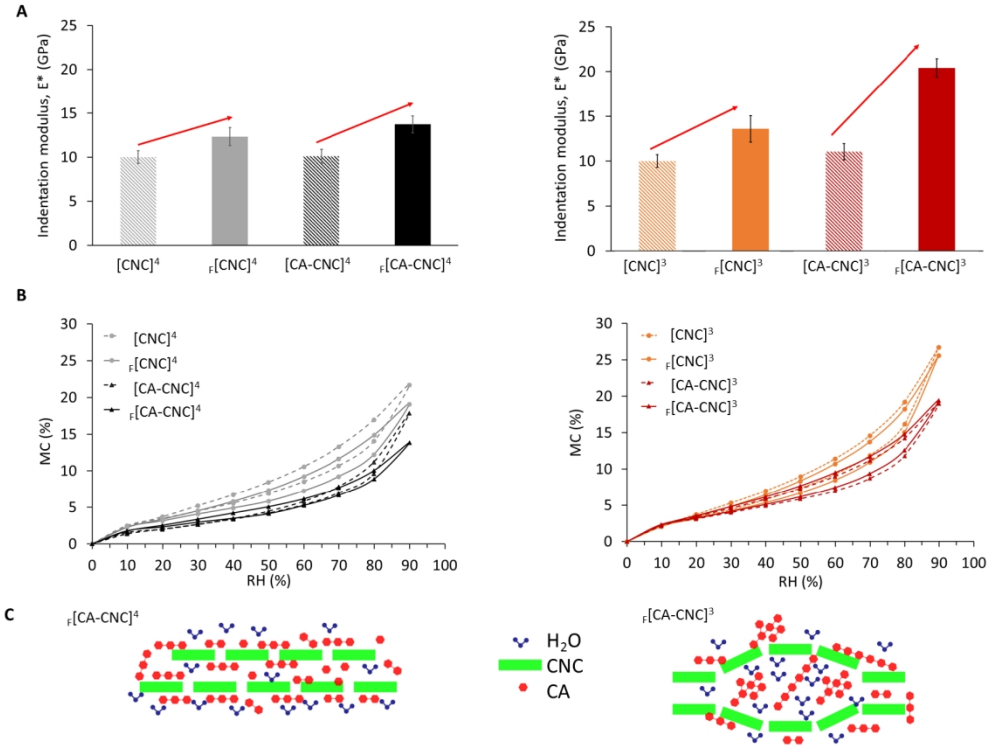


178x137mm (252 x 252 DPI)

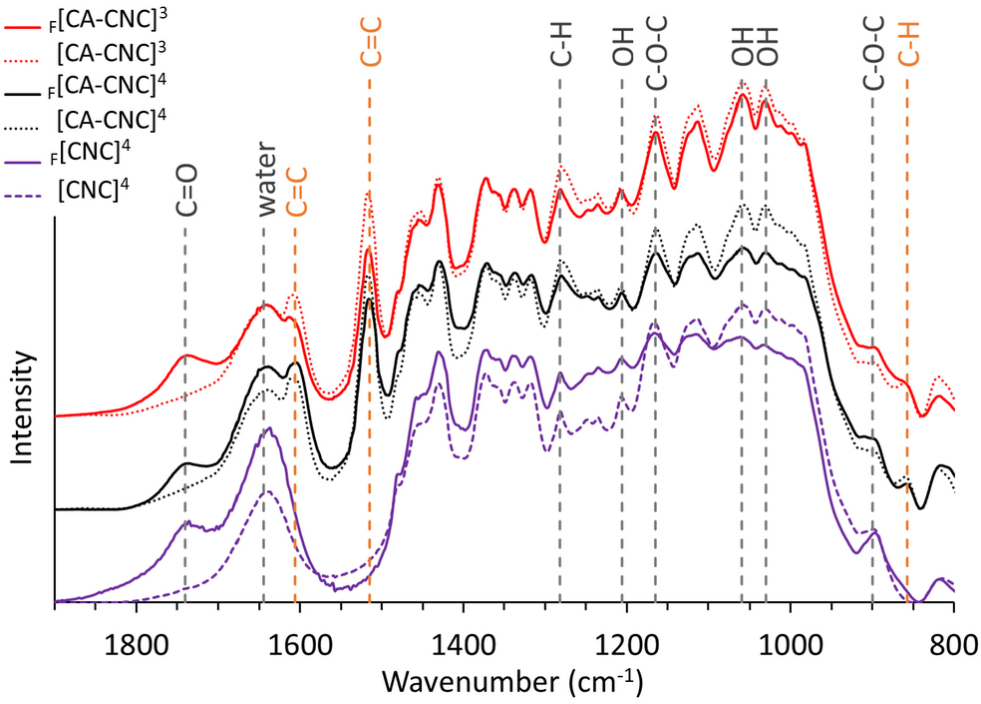


84x61mm (300 x 300 DPI)

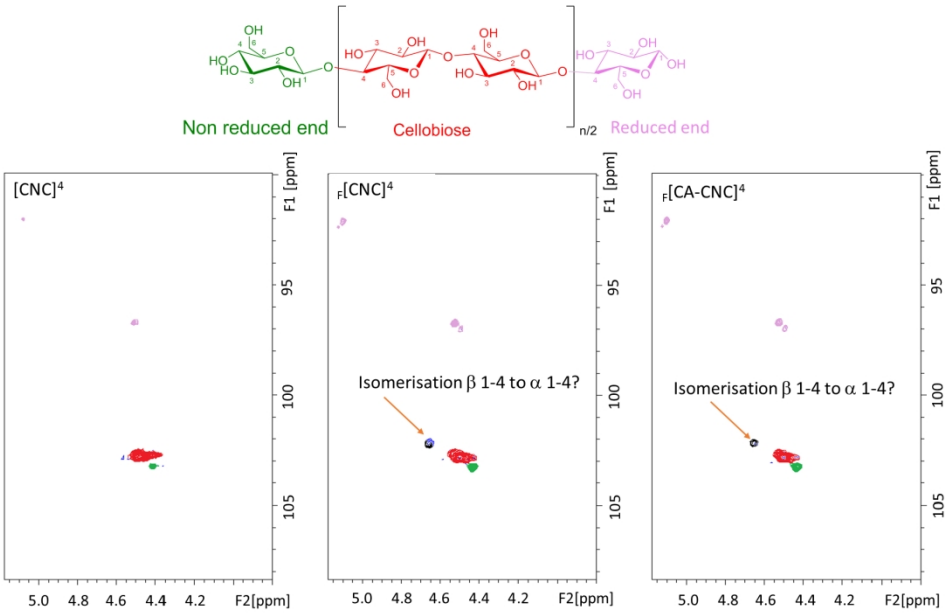


178x115mm (286 x 286 DPI)

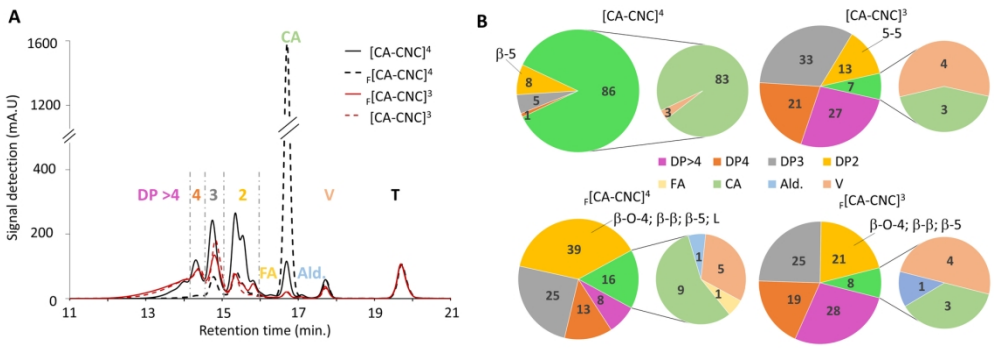


168x59mm (300 x 300 DPI)

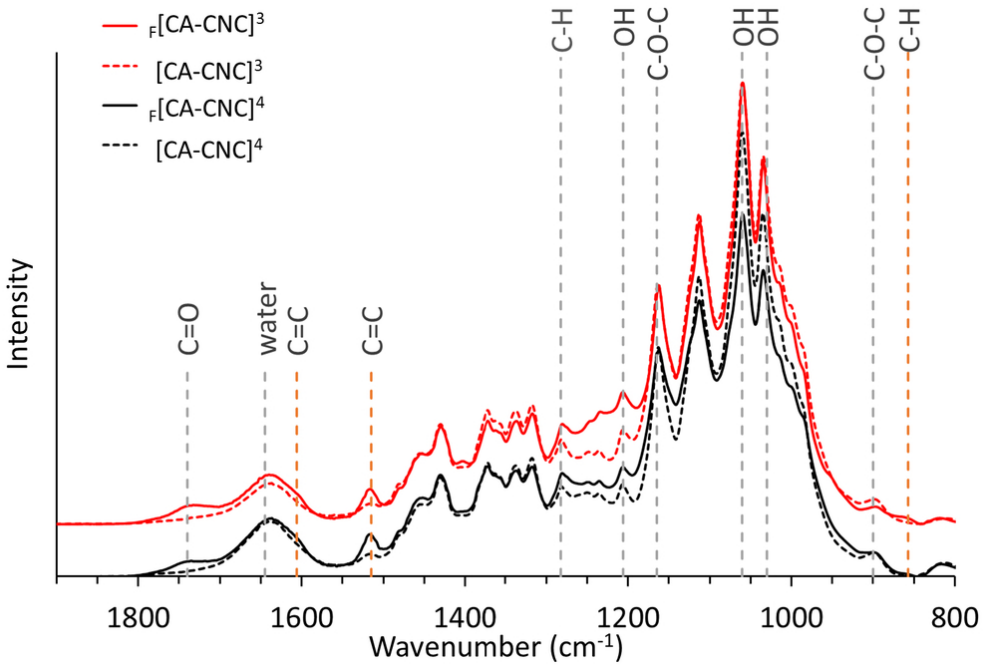


84x58mm (300 x 300 DPI)

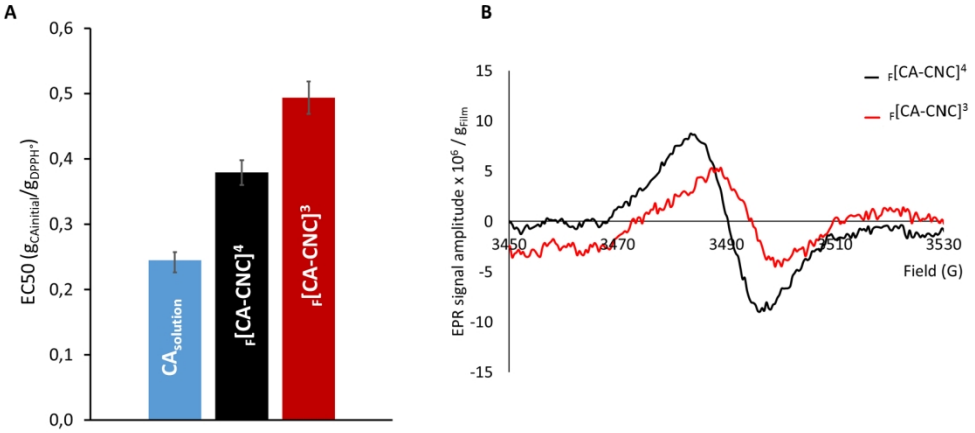


178x82mm (263 x 263 DPI)

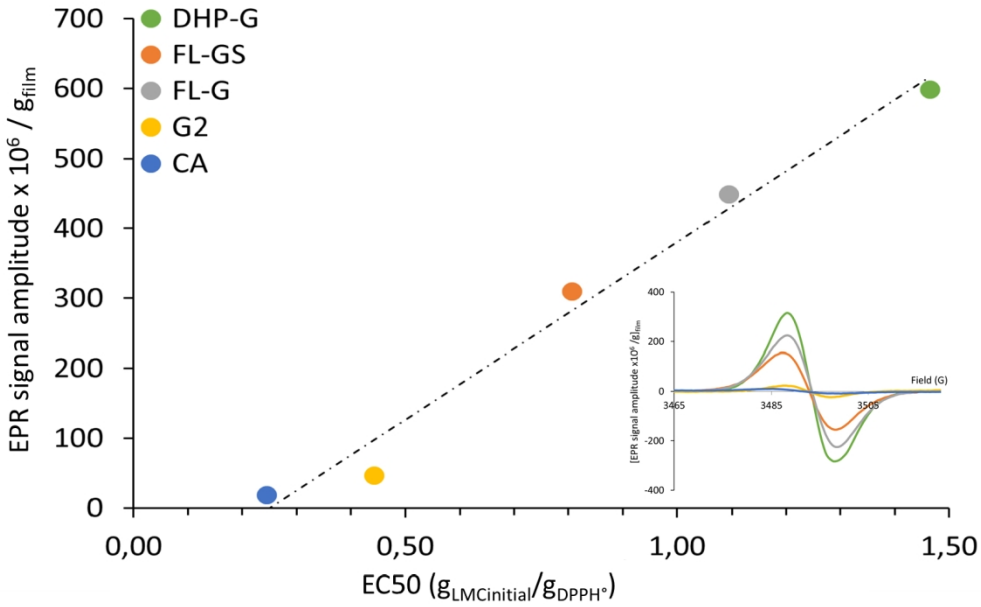


178x117mm (241 x 241 DPI)